Eur. Phys. J. C (2024) 84:304
https://doi.org/10.1140/epjc/s10052-024-12618-8

THE EUROPEAN PHYSICAL JOURNAL C

Regular Article - Theoretical Physics

Third-family lepton-quark *fusion*

Arman Korajac[1,a], **Peter Krack**[2,3,b], **Nudžeim Selimović**[4,c]

[1] J. Stefan Institute, Jamova 39, P. O. Box 3000, 1001 Ljubljana, Slovenia
[2] Department of Physics and Astronomy, Vrije Universiteit, 1081 HV Amsterdam, The Netherlands
[3] Nikhef Theory Group, Science Park 105, 1098 XG Amsterdam, The Netherlands
[4] Sezione di Padova, Istituto Nazionale di Fisica Nucleare, Via Francesco Marzolo 8, 35131 Padova, Italy

Received: 5 December 2023 / Accepted: 25 February 2024 / Published online: 23 March 2024

Abstract We analyze the signatures of new physics scenarios featuring third-family quark-lepton unification at the TeV scale in lepton-quark fusion at hadron colliders. Working with complete UV dynamics based on the $SU(4)$ gauge symmetry in the third-family fermions, we simulate the resonant production of a vector leptoquark at the next-to-leading order, including its decay and matching to the parton showers. The precise theoretical control over this production channel allows us to set robust bounds on the vector leptoquark parameter space which are complementary to the other production channels at colliders. We emphasize the importance of the resonant channel in future searches and discuss the impact of variations in the model space depending on the flavor structure of the vector leptoquark couplings.

1 Introduction

The experiments probing the Standard Model (SM) at different energies impose considerable constraints on new physics (NP) models addressing the Higgs hierarchy problem at the TeV scale. Notably, the present high-energy bounds on NP show significant variations depending on the flavor structure of possible new states. In particular, if the new states couple universally to the SM fermions with $\mathcal{O}(1)$ couplings, searches at the Large Hadron Collider (LHC) push their mass in the multi-TeV range. On the contrary, if the new states are primarily coupled to the third family, the LHC bounds on their mass become prominently weaker, often not surpassing 1 TeV [1]. The flavor structure of such NP, mainly coupled to the third family, evokes the connection to the hierarchical SM Yukawa couplings that, to a first approximation, can be described by nonvanishing entries corresponding to the interactions of the Higgs with the third-family fermions. Consequently, such a flavor non-universal NP could be a first step in addressing the SM flavor puzzle. Furthermore, linking NP at the TeV scale to the solution of the Higgs hierarchy problem opens as an enticing possibility.

The recent study in [2] provided a comprehensive investigation of NP models to elucidate the emergence of flavor hierarchies within a flavor non-universal gauge framework. It was found that, in order to mitigate significant quantum corrections to the Higgs mass, being consistent with the "finite naturalness" criterion [3], it is crucial for the initial layer of non-universality distinguishing the third family from the lighter families, to manifest itself at the TeV scale. Moreover, adding further criteria encompassing consistency with experimental data, and semi-simple embedding in the ultraviolet, filtered out a few models as possible SM extensions. Remarkably, all viable models exhibit quark-lepton unification within the third family together with a non-universal electroweak sector.

The possible intermediate step, before reaching the SM, common to all the phenomenologically viable models featuring the third-family quark-lepton unification is the so-called 4321 gauge group, $\mathcal{G}_{4321} = SU(4)_3 \times SU(3)_{12} \times SU(2)_L \times U(1)_X$, at the TeV scale [4,5]. The subscripts in $SU(4)_3 \times SU(3)_{12}$ denote the flavor non-universal scenario and indicate that the would-be third-family fermions are charged under $SU(4)_3$, while light families are charged under $SU(3)_{12}$. The gauge group $SU(2)_L$ is flavor universal and acts as in the SM, while $U(1)_X$ coincides with the SM hypercharge for light families and T_R^3 for the third family.

Aside from its theoretical appeal in providing a way to address the SM flavor puzzle and the Higgs hierarchy problem [6–9], the quark-lepton unification of this type necessarily involves a TeV-scale U_1 vector leptoquark mainly cou-

[a] e-mail: arman.korajac@ijs.si
[b] e-mail: peter.krack@nikhef.nl (corresponding author)
[c] e-mail: nudzeim.selimovic@pd.infn.it

pled to the third family. Indeed, such a field has been recognized as a solution for the experimental hints of Lepton Flavor Universality (LFU) violation in semileptonic B-meson decays with a charged current ($b \to c\tau\nu$) underlying quark transition [10–17]. Moreover, it could explain tensions in B-meson branching ratios and differential distributions [18–26] through a non-standard LFU contribution to a neutral current ($b \to s\ell\ell$) amplitude [27–30]. In this context, thorough studies of the implications of addressing B-anomalies via U_1 for $\Delta F = 1$ (including the impact in $B \to K\nu\bar{\nu}$ transitions, interesting in light of the recent Belle II measurement [31]) and $\Delta F = 2$ transitions [32–34], τ decays [35], and electroweak precision observables (EWPO) [36], revealed consistency with $\mathcal{G}_{4321}$ being at the TeV scale.

Regarding the direct probes of leptoquark states at the LHC, experimental collaborations rely on three well-established processes. First, there is a leptoquark pair production in a gg or a $q\bar{q}$ fusion via strong interactions, or a lepton exchange in t-channel [37,38]. Being strongly phase-space suppressed, a leptoquark pair production is not optimal for heavy leptoquark searches. Second, there is a single leptoquark plus lepton production in a quark-gluon scattering [39–42]. It suffers less phase-space suppression, and for $\mathcal{O}(1)$ couplings, it surpasses pair production. Third, a non-resonant t-channel leptoquark exchange in a Drell-Yan process could manifest as a deviation in the high-p_T tail of the dilepton invariant mass distribution [43–51]. In the limit of large couplings and masses beyond the kinematical reach for on-shell production, this process outweighs the other two. For recent experimental results, we refer the reader to [52–55].

In addition to the aforementioned search strategies, there has been a recent interest in the resonant leptoquark production from a direct lepton-quark fusion. The initial idea was put forth in [56], while practical implementations became possible only after the precise determination of lepton parton distribution functions (PDFs) inside the proton [57–61]. The suppression from lepton PDFs is compensated by the least phase-space suppression, making this channel competitive with other production mechanisms. Indeed, the previous work on this topic concerning scalar leptoquarks [62] showed that the lepton-quark fusion channel should be utilized as a complementary probe in parameter regions with $\mathcal{O}(1)$ leptoquark couplings and TeV-scale masses. Interestingly, this parameter region coincides with the one for the U_1 leptoquark in 4321 constructions, calling for a detailed analysis of this production channel in a complete UV model.

In fact, an analysis has been performed at leading order (LO) in the NP coupling, where the authors examined the resonant U_1 production at the LHC and its exclusion power on the U_1 parameter space [63]. At the time of conducting this analysis, no experimental searches for the resonant leptoquark production were available, hence the limits were derived using Monte Carlo-generated samples. Additionally, the signal events were showered by `Pythia` [64] which at present does not handle initial-state radiation from leptons. To circumvent this issue, initial leptons were substituted for photons in the `MadGraph` [65] generated LHE files [66].

We expand on this study in three ways. First, we calculate the NLO QCD + QED corrections to the U_1 production cross-section. Second, we match to `Herwig` which has an implemented lepton-showering algorithm [67] via the `POWHEG` method [68]. A study involving scalar leptoquarks [62] found that a proper treatment of initial-state radiation by leptons introduces an approximate 15% difference with respect to the particle label manipulation as is the case with `Pythia` in [63]. Finally, the CMS collaboration recently reported the first search for leptoquarks produced in a lepton-quark collision [69], which we utilize to find exclusion limits on the U_1 leptoquark coupling for different values of its mass.

The paper is structured as follows: In Sect. 2, we explain the 4321 model and the $\mathcal{G}_{4321} \to$ SM breaking pattern. We derive the relevant U_1 leptoquark Lagrangian and discuss its flavor structure. In Sect. 3, we present the details of the NLO calculation. Finally, Sect. 4 is devoted to a phenomenological study from which we derive the bounds on the U_1 parameters using the lepton-quark fusion channel.

2 The model

The model we consider is based on the $\mathcal{G}_{4321}$ gauge group and the matter content with transformation properties shown in Table 1. The gauge bosons associated with $SU(4)_3 \times SU(3)_{12} \times SU(2)_L \times U(1)_X$ dynamics are denoted by H_μ^A,

Table 1 Field content and charges under the $\mathcal{G}_{4321} = SU(4)_3 \times SU(3)_{12} \times SU(2)_L \times U(1)_X$ gauge group. The index $i = 1, 2$ labels the light fermion families, and $\psi_L \equiv (q_L^3\ \ell_L^3)^\intercal$, $\psi_R^+ \equiv (u_R^3\ \nu_R^3)^\intercal$ and $\psi_R^- \equiv (d_R^3\ e_R^3)^\intercal$ are multiplets unifying quarks and leptons of the third family

Field	$SU(4)_3$	$SU(3)_{12}$	$SU(2)_L$	$U(1)_X$
ψ_L	**4**	**1**	**2**	0
ψ_R^+	**4**	**1**	**1**	1/2
ψ_R^-	**4**	**1**	**1**	−1/2
q_L^i	**1**	**3**	**2**	1/6
ℓ_L^i	**1**	**1**	**2**	−1/2
u_R^i	**1**	**3**	**1**	2/3
d_R^i	**1**	**3**	**1**	−1/3
e_R^i	**1**	**1**	**1**	−1
H	**1**	**1**	**2**	1/2
Ω_3	$\bar{\mathbf{4}}$	**3**	**1**	1/6
Ω_1	$\bar{\mathbf{4}}$	**1**	**1**	−1/2

C^a_μ, W^I_μ, and X_μ, respectively. The corresponding adjoint indices are $A = 1, \ldots, 15$, $a = 1, \ldots, 8$, and $I = 1, 2, 3$, while the corresponding gauge couplings are g_4, g_3, g_2, and g_1.

The spontaneous symmetry breaking of $\mathcal{G}_{4321}$ to $\mathcal{G}_{\rm SM} = SU(3) \times SU(2)_L \times U(1)_Y$ results from the vacuum expectation values of two scalars Ω_3 and Ω_1 whose transformation properties under $\mathcal{G}_{4321}$ are shown in Table 1. The vacuum direction is such that $\mathcal{G}_{\rm SM} \supset SU(3) \times U(1)_Y = [SU(4)_3 \times SU(3)_{12} \times U(1)_X]_{\rm diag}$, and the hypercharge is given by $Y = X + \sqrt{2/3}\, T^{15}_4$, where $T^{15}_4 = \frac{1}{2\sqrt{6}}{\rm diag}(1, 1, 1, -3)$ is the $SU(4)_3$ generator. The massive gauge bosons resulting from the $\mathcal{G}_{4321} \to \mathcal{G}_{\rm SM}$ breaking include the coloron G', the U_1 vector leptoquark, and the neutral Z', which transform under $\mathcal{G}_{\rm SM}$ as $G' \sim (\mathbf{8}, \mathbf{1}, 0)$, $U_1 \sim (\mathbf{3}, \mathbf{1}, 2/3)$, and $Z' \sim (\mathbf{1}, \mathbf{1}, 0)$. They correspond to the following linear combinations of the $\mathcal{G}_{4321}$ gauge eigenstates

$$\begin{aligned} G'^a_\mu &= c_3 H^a_\mu - s_3 C^a_\mu, \quad Z'_\mu = c_1 H^{15}_\mu - s_1 X_\mu, \\ U^{1,2,3}_\mu &= \frac{1}{\sqrt{2}}(H^{9,11,13}_\mu - i H^{10,12,14}_\mu), \end{aligned} \tag{1}$$

where the mixing angles are $\theta_1 = \arctan(\sqrt{2/3}\, g_1/g_4)$, $\theta_3 = \arctan(g_3/g_4)$, and we used $c_{1,3} \equiv \cos\theta_{1,3}$ and $s_{1,3} \equiv \sin\theta_{1,3}$. The masses they obtain read

$$m_U = \frac{1}{2} g_4 f_U, \quad m_{Z',G'} = \frac{m_U}{c_{1,3}} \frac{f_{Z',G'}}{f_U}, \tag{2}$$

where $f^2_U = \omega^2_1 + \omega^2_3$, $f^2_{Z'} = 3\omega^2_1/2 + \omega^2_3/2$, $f^2_{G'} = 2\omega^2_3$, and $\omega_{1,3}$ denote the vacuum expectation values of $\Omega_{1,3}$. The field combinations orthogonal to G' and Z' in Eq. (1) correspond to the SM gluons, G^a_μ, and the hypercharge gauge boson, B_μ,

$$\begin{aligned} G^a_\mu &= (s_3\, H^a_\mu + c_3\, C^a_\mu),\ g_s = g_3\, c_3 = g_4\, s_3, \\ B_\mu &= (s_1\, H^{15}_\mu + c_1\, X_\mu),\ g_Y = g_X\, c_1 = \sqrt{\frac{3}{2}} g_4\, s_1, \end{aligned} \tag{3}$$

where we also expressed the QCD coupling, g_s, and the hypercharge coupling g_Y in terms of $\mathcal{G}_{4321}$ gauge couplings and mixing angles.

In this paper, we are interested in the production of U_1 leptoquark by lepton-quark fusion at hadron colliders, taking into account the NLO corrections from its interactions with gluons and photons. Thus, the relevant interactions for our purpose are described by the following Lagrangian

$$\begin{aligned} \mathcal{L}_{U_1} \supset\ & \frac{g_4}{\sqrt{2}} U_\mu \left(\beta^{i\alpha}_L\, \overline{q}^i_L \gamma^\mu \ell^\alpha_L + \beta^{i\alpha}_R\, \overline{q}^i_R \gamma^\mu \ell^\alpha_R + {\rm h.c.} \right) \\ & - i g_s U^\dagger_\mu T^a U_\nu G^{a,\mu\nu} - \frac{2}{3} i e\, U^\dagger_\mu U_\nu F^{\mu\nu}, \end{aligned} \tag{4}$$

where $G^a_{\mu\nu}$ and $F_{\mu\nu}$ are the gluon and the photon field strength tensors, and e is the QED coupling. The couplings to the left- and right-handed fermions β_L and β_R are 3×3 matrices in the quark-lepton family space that encode the flavor structure of the U_1 interactions. In the minimal version of the model, the U_1 couples to the third-family fermions only with $|\beta^{33}_{L,R}| = 1$, resulting in the exact $U(2)^5$ flavor symmetry of its interactions. However, in more realistic models, one expects populating the other entries of β_L following the $U(2)^5$ symmetry breaking [70,71]. The low-energy phenomenology of the U_1 leptoquark constrains the size of this breaking, pointing to suppression in the β_L entries parametrizing the couplings to light-family fields [33,34,71]. Thus, a dominant resonant production of the U_1 proceeds through the $b + \tau$ collisions, as the PDF enhancement from lighter quarks is insufficient to compensate for their suppressed couplings to U_1. In Sect. 4.3, we have explicitly checked that turning on couplings to light families compatible with all constraints leads to a negligible change in the exclusion bounds in the U_1 parameter space. Nevertheless, in the Monte Carlo tool we built, we keep $\beta_{L,R}$ as generic matrices and allow users to choose any values in order to match to other model implementations.

3 U_1 leptoquark resonant production @ NLO

In order to characterize the U_1 vector leptoquark production in lepton-quark collisions as precisely as possible, we rely on the Monte Carlo tool developed in [62]. In short, it is a `POWHEG-BOX-RES` implementation of the resonant leptoquark production apt of generating events which are processed by `Herwig` in order to obtain a full simulation of the collision at the NLO+PS level. We refer to Ref. [62] for the details of the implementation, reminding that in general, it requires the computation of the averaged matrix-squared elements for all real-radiation contributions, and the finite part of the virtual corrections computed in $\overline{\rm MS}$ scheme.

In the following, we summarize the necessary ingredients specific for the case of U_1 vector leptoquark originating from $\mathcal{G}_{4321}$ symmetry breaking. First, the partonic Born cross-section for $q^i + \ell^\alpha \to U_1$ is given as

$$\hat{\sigma}_{\rm LO} = \frac{g^2_4}{4} (|\beta^{i\alpha}_L|^2 + |\beta^{i\alpha}_R|^2)\, m^2_U. \tag{5}$$

Second, the NLO QCD effects affecting the U_1 leptoquark production by lepton-quark fusion consist of real-radiation corrections involving: the gluon-initiated production, $g(p_1) + \ell(p_2) \to q(k) + U_1(q)$ in Fig. 1a, and the soft-gluon emission, $q(p_1) + \ell(p_2) \to g(k) + U_1(q)$ in Fig. 1b, where the four-momenta of the particles are in the parentheses. The averaged matrix-squared element for the two processes read

$$|\overline{\mathcal{M}}|^2_{g\ell} = -\frac{1}{2} g^2_s g^2_4 \frac{s(s^2 + t^2 + 2u\, m^2_U)}{t(s+t)^2}, \tag{6}$$

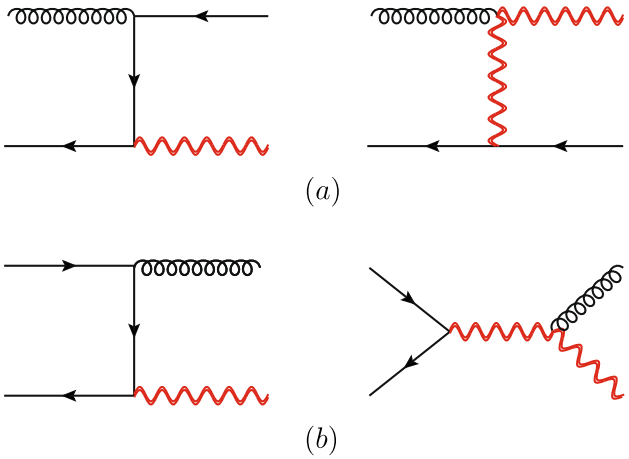

Fig. 1 Real-radiation QCD corrections: **a** gluon-initiated production $g + \ell \to q + U_1$; **b** gluon emission $q + \ell \to g + U_1$. The U_1 vector leptoquark is shown in red

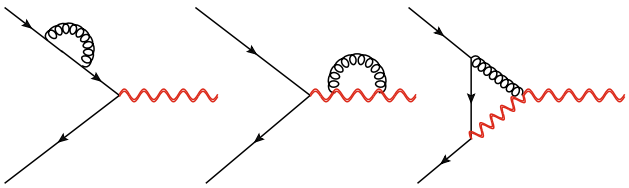

Fig. 2 Virtual QCD corrections: quark and U_1 leg corrections, and the vertex correction. The U_1 vector leptoquark is shown in red

$$|\overline{\mathcal{M}}|^2_{q\ell} = \frac{4}{3} g_s^2 g_4^2 \frac{u(u^2+t^2+2sm_U^2)}{t(u+t)^2}, \tag{7}$$

where s, t, and u are the partonic-level Mandelstam variables defined as $s = (p_1 + p_2)^2$, $t = (p_1 - k)^2$, $u = (p_1 - q)^2$, and we kept only the U_1 mass m_U.

Third, there are virtual QCD corrections originating from diagrams in Fig. 2. The details of evaluating the virtual NLO QCD corrections are presented in [72]. The finite part of the virtual corrections computed in dimensional regularization that needs to be provided to POWHEG [68] reads

$$\mathcal{V}_{\text{fin}} = \frac{2}{3} g_4^2 s \left(\frac{13}{12} - \frac{4\pi}{\sqrt{3}} + \frac{\pi^2}{2} - \frac{5}{2} L_R - \frac{1}{2} L_R^2 \right), \tag{8}$$

where $L_R = \log(\mu_R^2/s)$, and μ_R is the renormalization scale. We note that consistently evaluating these corrections involves the effects of coloron states, G'^a, specific to the full model implementation. Here, we assumed that coloron and U_1 leptoquark are mass degenerate. We have also checked that taking the extreme case $m_{G'} = \sqrt{2}\, m_U$, see Eq. (2), has a negligible impact on our results.

In addition to the corrections that originate from the U_1 interactions with gluons, there are QED corrections to the resonant leptoquark production from the process initiated by the photon. Specifically, $\gamma(p_1) + q(p_2) \to \ell(k) + U_1(q)$ in Fig. 3, contributes at the same order as the QCD corrections due to photon to lepton PDF enhancement compensating for the α_s to α_{QED} suppression. The averaged matrix-squared element for this process reads

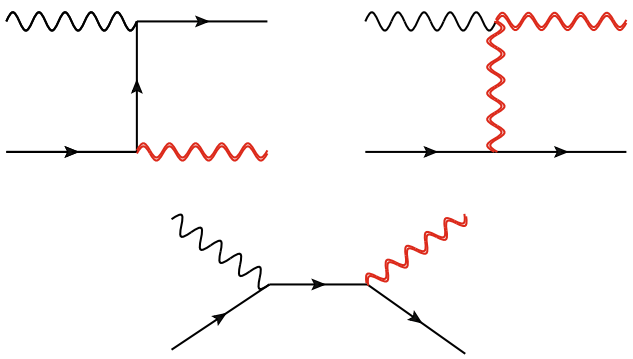

Fig. 3 Real-radiation QED corrections $\gamma + q \to \ell + U_1$. The photon/lepton PDF enhancement compensates for the α_{QED}/α_s suppression. The U_1 vector leptoquark is shown in red

$$|\overline{\mathcal{M}}|^2_{\gamma q} = -e^2 g_4^2 \left(\frac{Q_\ell s + Q_{\text{q}} t}{s+t} \right)^2 \frac{s^2+t^2+2u\,m_U^2}{st}, \tag{9}$$

where Q_ℓ and Q_{q} are lepton and quark electric charges, respectively. We note that the reported matrix elements should be divided by $\alpha_s/2\pi$ to adapt to the POWHEG input [68]. Additionally, in order to study a more general flavor structure, Eqs. (6)–(9) should be multiplied by $(|\beta_L^{i\alpha}|^2 + |\beta_R^{i\alpha}|^2)/2$, and the sum over all quark and lepton flavor combinations participating in the production should be taken.

Furthermore, we have used the derived averaged matrix elements to perform the analytic computation of the partonic cross-section for the U_1 production. The computation resembles the one for the case of the scalar leptoquark in Ref. [73] and we here give a way to translate those results to the case of the U_1. In addition to the universal replacement $y_{q\ell} \to g_4$, we find for the gluon-lepton collision the following partonic cross-section

$$\hat{\sigma}^{\text{vec}}_{g\ell} = 2\hat{\sigma}^{\text{sca}}_{g\ell} + \frac{\pi z g_4^2}{2m_U^2} \frac{\alpha_s}{2\pi} T_R \frac{2(1-z)}{z}, \tag{10}$$

where $\hat{\sigma}^{\text{sca}}_{g\ell}$ can be found in Eq. (2.4) in [73]. For the cross-section corrected by the virtual contributions and the real-gluon emission, we obtain

$$\hat{\sigma}^{\text{vec}}_{q\ell} = 2\hat{\sigma}^{\text{sca}}_{q\ell} - \frac{\pi z g_4^2}{2m_U^2} \frac{\alpha_s}{2\pi} C_F \left[\frac{2}{3}(1-z) + \left(\frac{2\pi^2}{3} - \frac{4\pi}{\sqrt{3}} + \frac{37}{12} - \frac{3}{2} L_R \right) \delta(1-z) \right], \tag{11}$$

where $\hat{\sigma}^{\rm sca}_{q\ell}$ corresponds to Eq. (2.3) in [73]. Finally, the partonic cross-section for the photon-initiated process reads

$$\hat{\sigma}^{\rm vec}_{\gamma\ell} = 2\hat{\sigma}^{\rm sca}_{\gamma\ell} + \frac{\pi z g_4^2}{2m_U^2}\frac{\alpha_{\rm QED}}{2\pi}\Bigg[4Q_{\rm q}Q_{\rm LQ}\log(z) + (Q_{\rm LQ}^2 + Q_{\rm q}^2 z)\frac{2(1-z)}{z}\Bigg], \tag{12}$$

where $Q_{\rm LQ}$ is the U_1 electric charge. In Eqs. (10)–(12), the variable $z = m_U^2/\hat{s}$ should be integrated over to obtain the hadronic cross-section

$$\sigma(s) = 2\sum_{ij}\int_\xi^1 dy\, f_i(y)\int_{\xi/y}^1 dz\,\frac{\xi}{yz^2} f_j\left(\frac{\xi}{yz}\right)\hat{\sigma}^{\rm vec}_{ij}. \tag{13}$$

The functions f_i and f_j correspond to the PDFs of i and j partons, $\xi = m_U^2/s$ with $\sqrt{s}$ being the collider center of mass energy, and y is the fraction of the proton momentum carried by the parton labeled by i. As before, to allow for different U_1 couplings, the expressions for $\hat{\sigma}^{\rm vec}$ should be multiplied by $(|\beta_L^{i\alpha}|^2 + |\beta_R^{i\alpha}|^2)/2$.

Let us also note that the impact of corrections due to new heavy dynamics proportional to $\alpha_4 = g_4^2/16\pi^2$ has been evaluated in [74]. Here, we assume that both parameters, m_U and g_4, are defined in the on-shell scheme with respect to the $\mathcal{O}(\alpha_4)$ corrections, such that the U_1 on-shell production does not receive any modification by definition. On the other hand, the non-trivial interplay between the low- and high-energy observables implies that U_1 contributions at low-energy will be modified by $\mathcal{O}(\alpha_4)$ corrections. For example, the preferred region for addressing the B-meson anomalies in the $g_4 - m_U$ plane will be modified in the presence of new heavy dynamics. We take this into account in our phenomenological analysis in Sect. 4.

Finally, we allow for the treatment of the finite-width effects which are especially important in the large g_4 regime. In particular, we assume that the only decay channels of U_1 are to massless fermions, such that its decay width reads

$$\Gamma = \frac{g_4^2}{48\pi} m_U \sum_{i,\alpha}\left(2\,|\beta_L^{i\alpha}|^2 + |\beta_R^{i\alpha}|^2\right). \tag{14}$$

We implement the effects of Γ during the generation of signal event samples by using the Breit–Wigner (BW) prescription for the U_1 propagator [75]. It approximates the $2 \to 2$ matrix element by adding an extra integration over the invariant mass which is spread around m_U according to the Breit–Wigner distribution [62]. In the code, this is achieved by setting the flag `BWgen` to 1 in the `POWHEG` input card. On the other hand, setting `BWgen` to 0 gives the narrow-width approximation (NWA) for the leptoquark resonance. As anticipated, for larger values of g_4, the finite-width effects become important, and $\sigma_{\rm BW}/\sigma_{\rm NWA} - 1 \simeq \mathcal{O}(1)$ already for $m_U \gtrsim 2.5$ TeV and $g_4 \sim 1.5$. Moreover, since the PDFs are convoluted with the BW weight inside the phase-space integral, larger widths allow for probing the lower Bjorken-x region of the PDFs. This region of the phase space compensates for the possible BW suppression, ultimately leading to a larger cross-section in comparison to the NWA estimate. Such effects regarding the breakdown of the NWA have already been pointed out in [76].

Table 2 Inclusive cross-section for the U_1 leptoquark produced by $b+\tau$ collisions at NLO QED + QCD. The first (second) uncertainty is from seven-point scale variations (PDF replicas)

m_U [TeV]	σ_{NLO} [pb]
0.50	$(2.67 \cdot 10^{-1})^{+1.41\%}_{-3.57\%} \pm 2.00\%$
1.00	$(1.14 \cdot 10^{-2})^{+1.11\%}_{-1.52\%} \pm 2.02\%$
1.50	$(1.29 \cdot 10^{-3})^{+1.06\%}_{-0.87\%} \pm 2.38\%$
2.00	$(2.20 \cdot 10^{-4})^{+1.05\%}_{-0.73\%} \pm 2.93\%$
2.50	$(4.69 \cdot 10^{-5})^{+1.09\%}_{-0.76\%} \pm 3.67\%$
3.00	$(1.14 \cdot 10^{-5})^{+1.15\%}_{-0.81\%} \pm 4.75\%$
3.50	$(3.01 \cdot 10^{-6})^{+1.39\%}_{-0.88\%} \pm 6.19\%$
4.00	$(8.27 \cdot 10^{-7})^{+1.82\%}_{-0.96\%} \pm 8.09\%$
4.50	$(2.32 \cdot 10^{-7})^{+2.07\%}_{-1.04\%} \pm 10.89\%$

4 Phenomenology

4.1 NLO inclusive cross section

As a first phenomenological study, we compute the inclusive hadronic cross-sections at NLO QCD + QED for the resonant vector leptoquark production in $b + \tau$ collisions at the LHC. We set the energy of the beams to 6.5 TeV each and use the `LUXlep-NNPDF31_nlo_as_0118_luxqed` PDF set, which has been obtained by combining the `NNPDF` 3.1 PDF set [77] together with the lepton PDFs reported in [57]. We scan over the relevant U_1 mass window, $m_U = [500, 5000]$ GeV, and the coupling is set to $g_4 = 1$. The entries of the β_R and β_L matrices are all set to zero with the exception of $\beta_L^{33} = \beta_R^{33} = 1$, and for practical purposes we abbreviate $\beta_{L,R}^{33} \equiv \beta_{L,R}$. The results reported in Table 2 are obtained in two ways. First, we integrate Eqs. (10)–(12) over the appropriate PDFs, as in Eq. (13). Second, we let `POWHEG` with the flag `BWgen 0` perform the phase-space integrals with the input provided in Sect. 3. The two methods agree perfectly, which serves as a cross-check of our results. To determine the scale uncertainties, we apply the typical seven-point scale variation, i.e. we set $\mu = \mu_R = \mu_F$ and then vary the two scales (μ_R the renormalization scale, and μ_F the factorization scale) by a factor of two. The uncertainty from the PDF set is estimated using the Monte Carlo replicas [77,78]. Replicas are PDFs fitted to pseudodata, which

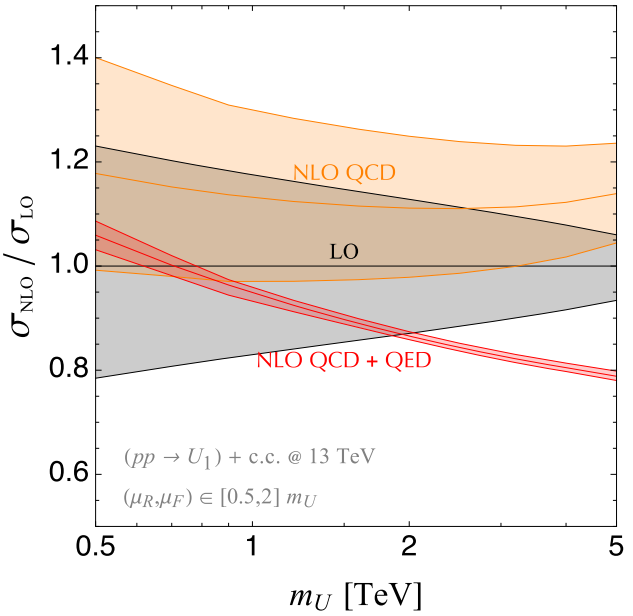

Fig. 4 NLO K-factors for the resonant vector leptoquarks production at $\sqrt{s} = 13$ TeV. The uncertainty bands were estimated using a seven-point scale variation

is generated randomly using a Gaussian distribution around each data point with the experimental uncertainty as variance. With the reweighting procedure in POWHEG-BOX, both the scale variations and the reweighting to the replicas, can be achieved for each generated event.

The NLO K-factors, defined as the ratio of the hadronic cross section after and before the NLO corrections, are plotted in Fig. 4. The central solid lines are obtained for $\mu_R = \mu_F = m_U$, while the bands reflect the scale uncertainties from the seven-point variation. The QCD corrections are positive and are mostly independent of the U_1 mass. On the other hand, the QED corrections are negative and larger than the QCD ones for $m_U \gtrsim 700$ GeV. What stands out is the cancellation of scale uncertainties when including both QCD and QED corrections, emphasizing the effect of the photon-initiated process in reducing the theoretical uncertainties. As can be seen from Table 2, the leading source of theoretical uncertainties is inadequate knowledge of the PDFs for large U_1 masses.

4.2 Differential distributions

In this subsection, we study differential distributions obtained from our simulation for the $b + \tau \to U_1$ leptoquark production. The most natural choice for the discriminating variable in resonant production searches is the invariant mass of the final states. In our case, the presence of the U_1 can be inferred through the invariant mass of the final jet-lepton system. We study the result for leading order and next-to-leading order events both before and after the parton shower. The mass is set to $m_U = 2000$ GeV and we use the same couplings as in Sect. 4.1. Therefore, the possible decay products of the U_1 leptoquark are $b + \tau$ or $t + \nu_\tau$. The events are passed to Herwig [67] for the parton shower and the anti-k_T algorithm from FastJet [79,80] is used for jet clustering. To enable the treatment of vector leptoquarks in Herwig, a suitable FeynRules [81] UFO-model needs to be used, e.g. [42,49,82–84].

In the benchmarks for the scalar leptoquarks reported in [62], the reconstruction was done by picking the hardest jet and lepton. This will still work before the parton shower, but not after, since the τ-lepton decays and produces a jet. A simple τ-tagging procedure is used: each jet close to a τ-lepton, with separation $\Delta R < 0.5$, is tagged with a static efficiency of 60%. However, just selecting the hardest τ-tagged jet and the hardest b-jet is not enough to reconstruct the leptoquarks mass adequately, since there is a significant amount of missing transverse momentum due to neutrinos produced in the τ-lepton decay. Therefore, we implement a simple recast analysis that relies on the cuts given in the mentioned CMS leptoquark search [69]. These cuts are selected to reduce most of the SM background events, characterized by softer radiation.

For the transverse momentum of the selected lepton or τ-tagged jet we set $p_T^\ell > 200$ GeV, and $p_T^j > 300$ GeV for the jet associated with the quark. A cut of $p_T^{miss} > 100$ GeV is set for the missing transverse momentum, and for the transverse momentum $p_T^{\ell+miss} > 100$ GeV of the $p_T^{miss} + p^\ell$ system. Rapidity cuts are set to $\eta_j < 2.4$ and $\eta_\ell < 2.1$. To capture the missing transverse momentum of the neutrinos produced during the τ decay, the azimuthal angle constraint between the visible part of the lepton and the missing p_T, $\Delta\phi_{\ell,miss} < 0.3$, is set. Moreover, the jets selected as the decay products of the leptoquark should be separated by demanding a cut on $\Delta R > 0.5$.

To reconstruct the mass of the leptoquark, we use the collinear mass defined as [69]

$$m_{\text{coll}} = m_{\text{vis}} \sqrt{\frac{p_T^{\text{vis}} + p_T^{\text{invis}}}{p_T^{\text{vis}}}}, \tag{15}$$

where p_T^{invis} is the part of p_T^{miss} in direction of the τ decay products. Since the decay of the τ-lepton is handled by Herwig, the quantity p_T^{invis} will only be non-zero for showered events. Therefore, if events are analyzed before the parton shower, the collinear mass corresponds to the invariant mass of the $b + \tau$ pair. All cuts mentioned above, as well as the couplings, can be modified in the POWHEG input card.

The resulting differential distribution, $d\sigma/dm_{\text{coll}}$, is shown in Fig. 5. A substantial difference is observed when the parton shower is turned on. In particular, after the parton shower, the τ-tagging and the additional cuts mentioned above cause

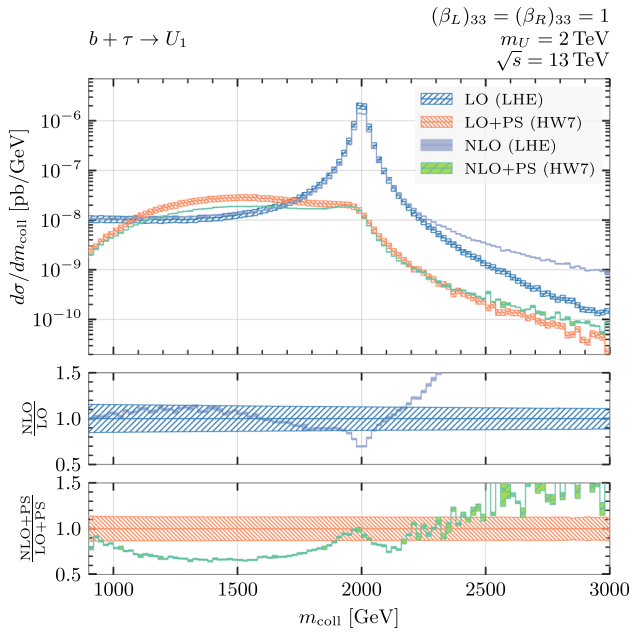

Fig. 5 Differential distribution for m_{coll} for the benchmark process described in Sect. 4 in the upper panel. The ratio NLO to LO of unshowered (showered) events is in the second (third) panel. The error bands were obtained using a seven-point scale variation. A τ-lepton is considered stable at the level of the LHE files, while its decay is implemented in the PS

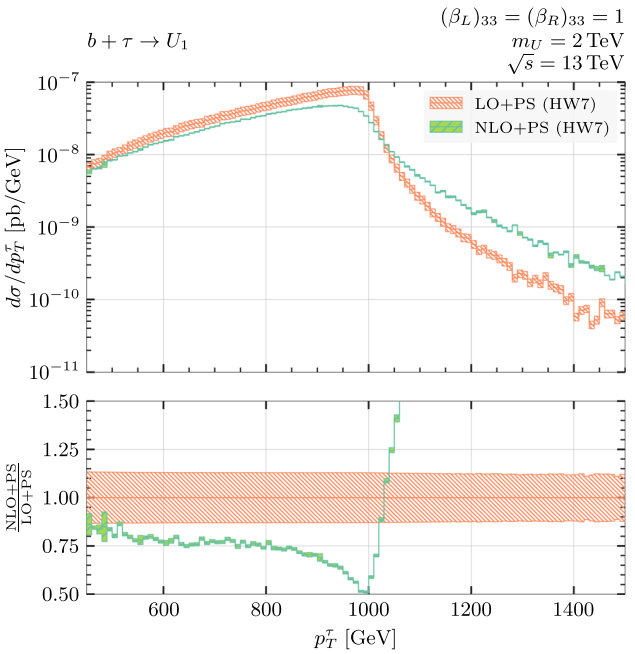

Fig. 6 Differential distribution for the transverse momentum of the tau-tagged jet with missing p_T and the ratio NLO to LO below. This quantity is only computed after the parton shower since the τ-lepton does not decay otherwise. The error bands were computed using the seven-point prescription for scale variation

fewer events to be reconstructed. Nevertheless, the differential cross-section is found to be larger after the shower for m_{coll} values below the peak. This is due to additional final-state radiation that lies outside the b- and τ-jet cones. The same effect also lowers the other tail of the distribution. Moreover, in the case of showered events, more jets are present, and the chance of misidentifying is higher. The NLO distribution, without the parton shower, has a broadened profile as a consequence of additional radiation in comparison to the leading order case. This slight depletion of the resonance peak can best be seen in the ratio subplot in Fig. 5.

As a different application of the code, in Fig. 6, we show the differential distribution of the transverse momentum for the tau-tagged jet. The missing p_T in the direction of the tau-tagged jet was added to obtain the expected Jacobian peak at $m_U/2 = 1000\,\text{GeV}$. Since finite-width effects were taken into account in our simulation, the peak is slightly smeared out. In the next-to-leading-order case, the extra radiation causes the leptoquark to have a non-zero transverse momentum, which causes the tail of the distribution above $m_U/2$ to be raised compared to the leading-order case.

We note that differential distributions for other kinematic quantities can easily be obtained by running the code.

4.3 LHC bounds

Given the available CMS search results [69] which, among others, target $b + \tau$ final states emerging from a scalar leptoquark LQ_s, we can establish constraints on the coupling strength g_4 in relation to the leptoquark mass m_U. The search relies on proton–proton collision data at a center-of-mass energy of $\sqrt{s} = 13$ TeV, obtained from the CMS detector, corresponding to an integrated luminosity of $\mathcal{L} = 138\,\text{fb}^{-1}$. To this end, it is necessary to highlight any potential differences that must be considered while applying this analysis to the U_1 signal. In general, the efficiency, i.e. the signal acceptance rate of the U_1 production for the cuts presented in Sect. 4.2 can be different. By performing a cut-and-count analysis for both scalar and vector leptoquark cases, we find that the efficiencies exhibit a minimal difference. This outcome is expected, given that the experimental search focuses on reconstructing signal events from the resonance peak, and other kinematical details become irrelevant.

The exclusion bounds, for different values of the scalar leptoquark coupling λ, are available on `HEPData` [85], where the coupling λ and the partonic cross-section for the scalar leptoquark production at LO are related as [62]

$$\hat{\sigma}_{\text{LQ}_s} = \frac{\lambda^2}{4} m^2_{\text{LQ}_s}. \tag{16}$$

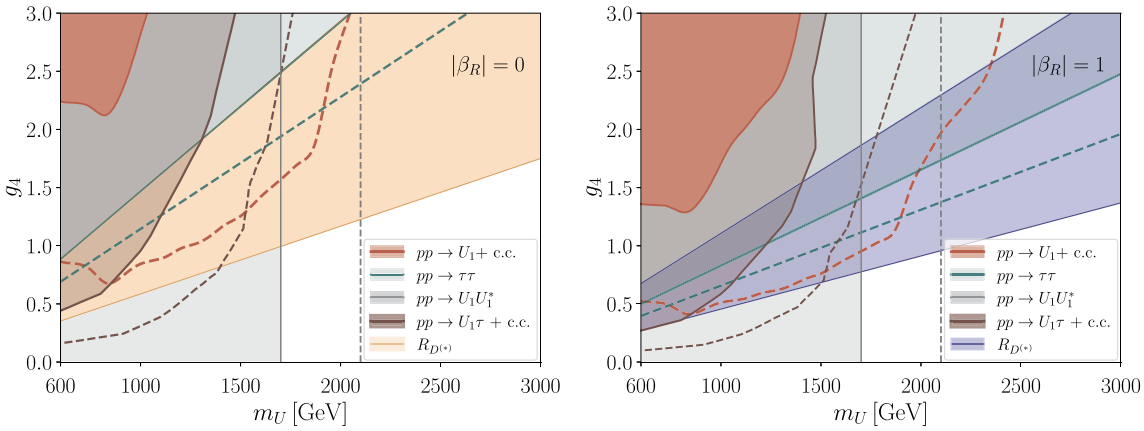

Fig. 7 Excluded parameter space at 95% CL for the U_1 resonant production from the observed limits, shown as the red region, in comparison to other production mechanisms. The bounds from $pp \to \tau\tau$ at 137 fb^{-1} derived by CMS [52], are depicted by the solid green line. The brown area is the excluded parameter space from the single leptoquark production [55]. The gray line corresponds to the exclusion limits set by the leptoquark pair production $pp \to U_1 U_1^\dagger$ [52]. The dashed lines represent the expected bounds, projected to 3 ab^{-1} for the c.o.m. energy $\sqrt{s} = 14$ TeV and follow the same color coding. In the left (right) panel, $|\beta_R|$ is set to zero (one), whereas $|\beta_L|$ equals 1 in both cases

The experimental sensitivity decreases for larger values of λ due to the increase in the leptoquark width, while the experimental resolution of m_{coll} is fixed. Therefore, we can directly translate the exclusion limits from the scalar to the vector leptoquark case, provided the widths are the same for both choices of couplings. This is achieved once the couplings (g_4, β_L, β_R) satisfy the following relation for a fixed λ

$$\lambda = \frac{g_4}{\sqrt{3}}\sqrt{2|\beta_L|^2 + |\beta_R|^2}. \tag{17}$$

We employ POWHEG to compute the U_1 production cross section at NLO, using the full BW prescription, and assume that the leptoquark solely couples to third-family fermions. We analyze two distinct cases, namely $|\beta_L| = |\beta_R| = 1$ and $|\beta_L| = 1, |\beta_R| = 0$, resulting in a fixed branching ratio of 68% (50%) for the first (second) choice. We note that in the latter case, the U_1 resonance is narrower compared to the scalar leptoquark case if we take $\lambda = g_4$. The slight improvement in sensitivity, however, is found to be negligible.

Calculating the cross-section for various points in the (g_4, m_U) parameter space, we can determine the values that saturate the imposed limits. In Fig. 7, we compare the bounds resulting from the resonant production of U_1 in $b+\tau$ fusion, and the bounds derived from alternative vector leptoquark production mechanisms for the choices $|\beta_L| = |\beta_R| = 1$ and $|\beta_L| = 1$, $|\beta_R| = 0$. The current exclusion bounds from lepton-quark fusion are obtained from translating the observed CMS bounds for the scalar leptoquarks as discussed above, and are shown in the red region in Fig. 7. The most stringent exclusions arise from the non-resonant effect of U_1 in $pp \to \tau\tau$ [86–88] shown in the green area. In the region of small leptoquark masses, the dominant bounds arise from the pair production [52] given by the gray area. Additionally, we display the bounds from $pp \to U_1\tau$, where the excluded portion of the parameter space is represented by the brown region. The dashed lines represent projections of the expected bounds at the high-luminosity LHC phase (HL-LHC) reaching $\mathcal{L} = 3\,\text{ab}^{-1}$ with the center-of-mass energy $\sqrt{s} = 14$ TeV [89]. For the derivation of these bounds, we consider that the experimental uncertainty is dominated by statistics, hence the sensitivity scales with the square root of the luminosity. The projected limits for the single production channel are extrapolated assuming the same sensitivity for masses above $m_U > 1600$ GeV as for $m_U = 1600$ GeV, given in [55]. The lepton-quark fusion projections improve better relative to the single production ones owing to the larger discrepancy between observed and expected limits in the former production channel [55,69].

Apart from the exclusion bounds comparison, we also check the sensitivity of the resonant channel to the 90% CL preferred region addressing the hints of LFU violation in the observables R_D and R_{D^*} [88]. As can be seen, the lepton-quark fusion will help to scrutinize the low-energy parameter space preferred by the charged-current B-meson anomalies during the HL-LHC.

Although the present $b+\tau$ fusion search does not exclude any additional part of the $g_4 - m_U$ parameter plane, the exclusion limits are competitive to other production mechanisms at the HL-LHC. Specifically, for $g_4 \gtrsim 1$, the resonant production channel outperforms the single production mechanism. When comparing to the non-resonant $pp \to \tau\tau$ process, it is important to note that the sensitivities scale differently with the luminosity, $\mathcal{L}$, improvement. For a fixed branching ratio, the resonant production cross-section scales with the coupling squared, which means that the bounds on the coupling

scale as $\mathcal{L}^{-1/4}$. In contrast, the bounds from $pp \to \tau\tau$ will improve by an approximate factor of $\mathcal{L}^{-1/8}$. Therefore, we emphasize the important role that the lepton-quark fusion will play during the HL-LHC: it provides complementary information about the U_1 leptoquark that experimental collaborations at the LHC should explore.

Finally, we note that phenomenologically allowed departures from the minimal model discussed here have a minuscule impact on the derived bounds. As an example, it is possible to achieve U_1 couplings to light-family fermions through mixing with additional fermion states which are vector-like under the SM gauge group [33]. In particular, a fit to low-energy observables in [90] prefers $\beta_L^{23} \simeq 0.2$, which results in an additional production channel for the U_1 leptoquark. We have checked that including such contribution from $s+\tau$ collisions results in an improvement of $\simeq 2.5\%$ in the exclusion bounds. In the case of other couplings, the situation is worse as the PDF enhancement for lighter quarks cannot compensate for the additional coupling suppression as dictated by the model's $U(2)^5$ protection and strong constraints on the light-family U_1 couplings. Thus, we expect the reported bounds to be robust to model modifications and represent a large class of models based on the $\mathcal{G}_{4321}$ gauge group.

5 Conclusions

The main objective of this work is to give a precise analysis of a direct $b + \tau$ fusion producing a vector leptoquark at the LHC. Such a state is part of the spectrum of NP constructions that feature third-family quark-lepton unification. Being interested in the NLO analysis, we work with a full UV model based on a flavor non-universal gauge group $\mathcal{G}_{4321}$ with an $SU(4)$ factor acting on the third-family fermions as in Table 1. As emphasized in the introduction, this class of models has been identified as a possible last step in breaking to the SM, of more ambitious models addressing the $U(2)^5$-like structure of the SM Yukawas, the electroweak scale stability, and the charge quantization problem.

After describing the gauge boson dynamics, we presented the results of NLO QCD + QED corrections for the partonic processes contained in $pp \to U_1$. We found that two corrections partially cancel, resulting in a smaller cross-section for a wide range of vector leptoquark masses, as shown in Fig. 4. Our computation led to a substantial reduction of the renormalization and factorization scale variation uncertainties, with the leading source of theoretical error being the limited knowledge of PDFs at large x, indicated in Table 2.

Following the implementation of the NLO results into `POWHEG`, together with the utilization of the parton + lepton showering algorithm offered by `Herwig`, we have effectively constructed a Monte Carlo event generator for this production channel. It can be obtained from the following Github repository https://github.com/peterkrack/3rd-Lepton-Quark-Fusion, and used to perform detailed phenomenological analyses by studying arbitrary differential distributions. As an example, we produced the distribution of events in a discriminating observable m_{coll} (see Eq. (15)) used in the CMS search for scalar leptoquarks in this channel [69]. Based on our findings, we were able to translate the CMS exclusion bounds for the scalar leptoquarks to the case of the U_1.

Despite the limiting exclusion power of the lepton-quark fusion channel at present, we have demonstrated that this channel will be prominent during the high-luminosity LHC phase. Owing to the resonant enhancement, the limits on the U_1 leptoquark parameter space from the lepton-quark fusion are more sensitive to luminosity and the center-of-mass energy improvements than the limits from the other channels, resulting in their full complementarity in Fig. 7. Our work provides the necessary ingredients on the theoretical side to make the best use of this, opening the possibility of performing the first experimental search for the U_1 vector leptoquark in the lepton-quark fusion channel.

Acknowledgements We thank Javier M. Lizana and Jernej F. Kamenik for useful discussions, and Admir Greljo for carefully reading the manuscript. This project has received funding from the INFN Iniziative Specifica APINE, the Slovenian Research Agency (grant No. J1-3013 and research core funding No. P1-0035), and the European Research Council (ERC) under the European Union's Horizon 2020 research and innovation programme under grant agreement 833280 (FLAY).

Data Availability Statement This manuscript has no associated data or the data will not be deposited. [Authors' comment: No datasets were generated in this work.]

Code availability This manuscript has associated code/software in a data repository. [Author's comment: The code is available in the repository: https://github.com/peterkrack/3rd-Lepton-Quark-Fusion.]

Funded by SCOAP[3].

References

1. L. Allwicher, C. Cornella, G. Isidori, B.A. Stefanek, New Physics in the Third Generation: A Comprehensive SMEFT Analysis and Future Prospects, 10 (2023)

2. J. Davighi, G. Isidori, Non-universal gauge interactions addressing the inescapable link between Higgs and flavour. JHEP **07**, 147 (2023)
3. M. Farina, D. Pappadopulo, A. Strumia, A modified naturalness principle and its experimental tests. JHEP **08**, 022 (2013)
4. L. Di Luzio, A. Greljo, M. Nardecchia, Gauge leptoquark as the origin of B-physics anomalies. Phys. Rev. D **96**(11), 115011 (2017)
5. A. Greljo, B.A. Stefanek, Third family quark–lepton unification at the TeV scale. Phys. Lett. B **782**, 131–138 (2018)
6. M. Bordone, C. Cornella, J. Fuentes-Martin, G. Isidori, A three-site gauge model for flavor hierarchies and flavor anomalies. Phys. Lett. B **779**, 317–323 (2018)
7. J. Fuentes-Martín, P. Stangl, Third-family quark-lepton unification with a fundamental composite Higgs. Phys. Lett. B **811**, 135953 (2020)
8. J. Fuentes-Martin, G. Isidori, J. Pagès, B.A. Stefanek, Flavor non-universal Pati-Salam unification and neutrino masses. Phys. Lett. B **820**, 136484 (2021)
9. J. Fuentes-Martin, G. Isidori, J.M. Lizana, N. Selimovic, B.A. Stefanek, Flavor hierarchies, flavor anomalies, and Higgs mass from a warped extra dimension. Phys. Lett. B **834**, 137382 (2022)
10. D. Buttazzo, A. Greljo, G. Isidori, D. Marzocca, B-physics anomalies: a guide to combined explanations. JHEP **11**, 044 (2017)
11. J.P. Lees et al., Evidence for an excess of $\bar{B} \to D^{(*)}\tau^-\bar{\nu}_\tau$ decays. Phys. Rev. Lett. **109**, 101802 (2012)
12. J.P. Lees et al., Measurement of an Excess of $\bar{B} \to D^{(*)}\tau^-\bar{\nu}_\tau$ Decays and Implications for Charged Higgs Bosons. Phys. Rev. D **88**(7), 072012 (2013)
13. M. Huschle et al., Measurement of the branching ratio of $\bar{B} \to D^{(*)}\tau^-\bar{\nu}_\tau$ relative to $\bar{B} \to D^{(*)}\ell^-\bar{\nu}_\ell$ decays with hadronic tagging at Belle. Phys. Rev. D **92**(7), 072014 (2015)
14. S. Hirose et al., Measurement of the τ lepton polarization and $R(D^*)$ in the decay $\bar{B} \to D^*\tau^-\bar{\nu}_\tau$ with one-prong hadronic τ decays at Belle. Phys. Rev. D **97**(1), 012004 (2018)
15. G. Caria et al., Measurement of $\mathcal{R}(D)$ and $\mathcal{R}(D^*)$ with a semileptonic tagging method. Phys. Rev. Lett. **124**(16), 161803 (2020)
16. R. Aaij et al., Measurement of the ratio of branching fractions $\mathcal{B}(\bar{B}^0 \to D^{*+}\tau^-\bar{\nu}_\tau)/\mathcal{B}(\bar{B}^0 \to D^{*+}\mu^-\bar{\nu}_\mu)$, Phys. Rev. Lett., vol. 115, no. 11, p. 111803 (2015). [Erratum: Phys.Rev.Lett. 115, 159901 (2015)]
17. R. Aaij et al., Measurement of $R_{D^{(*)}}$ with hadronic τ^+ decays at $\sqrt{s} = 13$ TeV by the LHCb collaboration
18. R. Aaij et al., Differential branching fractions and isospin asymmetries of $B \to K^{(*)}\mu^+\mu^-$ decays. JHEP **06**, 133 (2014)
19. R. Aaij et al., Measurements of the S-wave fraction in $B^0 \to K^+\pi^-\mu^+\mu^-$ decays and the $B^0 \to K^*(892)^0\mu^+\mu^-$ differential branching fraction, JHEP, **11**, 047 (2016). [Erratum: JHEP 04, 142 (2017)]
20. R. Aaij et al., Angular analysis and differential branching fraction of the decay $B_s^0 \to \phi\mu^+\mu^-$. JHEP **09**, 179 (2015)
21. R. Aaij et al., Differential branching fraction and angular analysis of $\Lambda_b^0 \to \Lambda\mu^+\mu^-$ decays, JHEP, **06**, 115 (2015). [Erratum: JHEP 09, 145 (2018)]
22. R. Aaij et al., Measurement of CP-Averaged Observables in the $B^0 \to K^{*0}\mu^+\mu^-$ Decay. Phys. Rev. Lett. **125**(1), 011802 (2020)
23. R. Aaij et al., Angular Analysis of the $B^+ \to K^{*+}\mu^+\mu^-$ Decay. Phys. Rev. Lett. **126**(16), 161802 (2021)
24. M. Aaboud et al., Angular analysis of $B_d^0 \to K^*\mu^+\mu^-$ decays in pp collisions at $\sqrt{s} = 8$ TeV with the ATLAS detector. JHEP **10**, 047 (2018)
25. Measurement of the P_1 and P_5' angular parameters of the decay $B^0 \to K^{*0}\mu^+\mu^-$ in proton-proton collisions at $\sqrt{s} = 8$ TeV, (2017)
26. S. Wehle et al., Lepton-Flavor-Dependent Angular Analysis of $B \to K^*\ell^+\ell^-$. Phys. Rev. Lett. **118**(11), 111801 (2017)
27. C. Bobeth, U. Haisch, New Physics in Γ_{12}^s: $(\bar{s}b)(\bar{\tau}\tau)$ Operators. Acta Phys. Polon. B **44**, 127–176 (2013)
28. A. Crivellin, C. Greub, D. Müller, F. Saturnino, Importance of Loop Effects in Explaining the Accumulated Evidence for New Physics in B Decays with a Vector Leptoquark. Phys. Rev. Lett. **122**(1), 011805 (2019)
29. A. Angelescu, D. Bečirević, D.A. Faroughy, O. Sumensari, Closing the window on single leptoquark solutions to the B-physics anomalies. JHEP **10**, 183 (2018)
30. G. Isidori, Z. Polonsky, A. Tinari, Semi-inclusive b→s$\ell^-\ell$ transitions at high q2. Phys. Rev. D **108**(9), 093008 (2023)
31. A. Glazov, Belle II physics highlights. plenary talk given at the EPS-HEP2023 Conference in Hamburg Germany, (2023)
32. L. Di Luzio, J. Fuentes-Martin, A. Greljo, M. Nardecchia, S. Renner, Maximal Flavour Violation: a Cabibbo mechanism for leptoquarks. JHEP **11**, 081 (2018)
33. J. Fuentes-Martín, G. Isidori, M. König, N. Selimović, Vector Leptoquarks Beyond Tree Level III: Vector-like Fermions and Flavor-Changing Transitions. Phys. Rev. D **102**, 115015 (2020)
34. O.L. Crosas, G. Isidori, J.M. Lizana, N. Selimovic, B.A. Stefanek, Flavor non-universal vector leptoquark imprints in $K \to \pi\nu\bar{\nu}$ and $\Delta F = 2$ transitions. Phys. Lett. B **835**, 137525 (2022)
35. L. Allwicher, G. Isidori, N. Selimovic, LFU violations in leptonic τ decays and B-physics anomalies. Phys. Lett. B **826**, 136903 (2022)
36. L. Allwicher, G. Isidori, J.M. Lizana, N. Selimovic, B.A. Stefanek, Third-family quark-lepton Unification and electroweak precision tests. JHEP **05**, 179 (2023)
37. A. Bessaa, S. Davidson, Constraints on t -channel leptoquark exchange from LHC contact interaction searches. Eur. Phys. J. C **75**(2), 97 (2015)
38. I. Dorsner, S. Fajfer, A. Greljo, Cornering Scalar Leptoquarks at LHC. JHEP **10**, 154 (2014)
39. A. Alves, O. Eboli, T. Plehn, Stop lepton associated production at hadron colliders. Phys. Lett. B **558**, 165–172 (2003)
40. J.B. Hammett, D.A. Ross, NLO Leptoquark Production and Decay: The Narrow-Width Approximation and Beyond. JHEP **07**, 148 (2015)
41. T. Mandal, S. Mitra, S. Seth, Single Productions of Colored Particles at the LHC: An Example with Scalar Leptoquarks. JHEP **07**, 028 (2015)
42. I. Doršner, A. Greljo, Leptoquark toolbox for precision collider studies. JHEP **05**, 126 (2018)
43. D.A. Faroughy, A. Greljo, J.F. Kamenik, Confronting lepton flavor universality violation in B decays with high-p_T tau lepton searches at LHC. Phys. Lett. B **764**, 126–134 (2017)
44. M. Schmaltz, Y.-M. Zhong, The leptoquark Hunter's guide: large coupling. JHEP **01**, 132 (2019)
45. A. Greljo, D. Marzocca, High-p_T dilepton tails and flavor physics. Eur. Phys. J. C **77**(8), 548 (2017)
46. J. Fuentes-Martin, A. Greljo, J. Martin Camalich, J.D. Ruiz-Alvarez, Charm physics confronts high-p$_T$ lepton tails, JHEP, **11**, 080 (2020)
47. A. Greljo, J. Martin Camalich, J.D. Ruiz-Álvarez, Mono-τ Signatures at the LHC Constrain Explanations of B-decay Anomalies, Phys. Rev. Lett., **122**(13), 131803 (2019)
48. D. Marzocca, U. Min, M. Son, Bottom-Flavored Mono-Tau Tails at the LHC. JHEP **12**, 035 (2020)
49. M.J. Baker, J. Fuentes-Martín, G. Isidori, M. König, High- p_T signatures in vector–leptoquark models. Eur. Phys. J. C **79**(4), 334 (2019)
50. U. Haisch, L. Schnell, S. Schulte, Drell-Yan production in third-generation gauge vector leptoquark models at NLO+PS in QCD. JHEP **02**, 070 (2023)
51. U. Haisch, L. Schnell, S. Schulte, On Drell-Yan production of scalar leptoquarks coupling to heavy-quark flavours. JHEP **11**, 106 (2022)

52. A.M. Sirunyan et al., Search for singly and pair-produced leptoquarks coupling to third-generation fermions in proton-proton collisions at s=13 TeV. Phys. Lett. B **819**, 136446 (2021)
53. Search for scalar leptoquarks in the $b\tau\tau$ final state in pp collisions at $\sqrt{s} = 13$ TeV with the ATLAS detector (2022)
54. G. Aad et al., Search for leptoquarks decaying into the $b\tau$ final state in pp collisions at $\sqrt{s}$ = 13 TeV with the ATLAS detector. JHEP **10**, 001 (2023)
55. A. Hayrapetyan et al., Search for a third-generation leptoquark coupled to a τ lepton and a b quark through single, pair, and non-resonant production in proton-proton collisions at $\sqrt{s}$ = 13 TeV, 8 (2023)
56. J. Ohnemus, S. Rudaz, T.F. Walsh, P.M. Zerwas, Single leptoquark production at hadron colliders. Phys. Lett. B **334**, 203–207 (1994)
57. L. Buonocore, P. Nason, F. Tramontano, G. Zanderighi, Leptons in the proton. JHEP **08**(08), 019 (2020)
58. A. Manohar, P. Nason, G.P. Salam, G. Zanderighi, How bright is the proton? A precise determination of the photon parton distribution function. Phys. Rev. Lett. **117**(24), 242002 (2016)
59. A.V. Manohar, P. Nason, G.P. Salam, G. Zanderighi, The Photon Content of the Proton. JHEP **12**, 046 (2017)
60. E.d.S. Almeida, A. Alves, O.J.P. Éboli, F.S. Queiroz, Resonant lepton-gluon collisions at the Large Hadron Collider, Phys. Rev. D, **107**(5), 055024 (2023)
61. S. Ajmal, J. Gaglione, A. Gurrola, O. Panella, M. Presilla, F. Romeo, H. Sun, S.-S. Xue, Searching for exclusive leptoquarks with the Nambu-Jona-Lasinio composite model at the LHC and HL-LHC, **11** (2023)
62. L. Buonocore, A. Greljo, P. Krack, P. Nason, N. Selimovic, F. Tramontano, G. Zanderighi, Resonant leptoquark at NLO with POWHEG. JHEP **11**, 129 (2022)
63. U. Haisch, G. Polesello, Resonant third-generation leptoquark signatures at the Large Hadron Collider. JHEP **05**, 057 (2021)
64. T. Sjöstrand, S. Ask, J.R. Christiansen, R. Corke, N. Desai, P. Ilten, S. Mrenna, S. Prestel, C.O. Rasmussen, P.Z. Skands, An introduction to PYTHIA 8.2. Comput. Phys. Commun. **191**, 159–177 (2015)
65. J. Alwall, R. Frederix, S. Frixione, V. Hirschi, F. Maltoni, O. Mattelaer, H.S. Shao, T. Stelzer, P. Torrielli, M. Zaro, The automated computation of tree-level and next-to-leading order differential cross sections, and their matching to parton shower simulations. JHEP **07**, 079 (2014)
66. L. Buonocore, U. Haisch, P. Nason, F. Tramontano, G. Zanderighi, Lepton-Quark Collisions at the Large Hadron Collider. Phys. Rev. Lett. **125**(23), 231804 (2020)
67. J. Bellm et al., Herwig 7.2 release note, Eur. Phys. J. C, vol. 80, no. 5, p. 452, (2020)
68. S. Alioli, P. Nason, C. Oleari, E. Re, A general framework for implementing NLO calculations in shower Monte Carlo programs: the POWHEG BOX. JHEP **06**, 043 (2010)
69. A. Hayrapetyan et al., Search for Scalar Leptoquarks Produced via τ-Lepton–Quark Scattering in pp Collisions at s=13 TeV. Phys. Rev. Lett. **132**(6), 061801 (2024)
70. R. Barbieri, G. Isidori, A. Pattori, F. Senia, Anomalies in B-decays and $U(2)$ flavour symmetry. Eur. Phys. J. C **76**(2), 67 (2016)
71. J. Fuentes-Martín, G. Isidori, J. Pagès, K. Yamamoto, With or without U(2)? Probing non-standard flavor and helicity structures in semileptonic B decays. Phys. Lett. B **800**, 135080 (2020)
72. J. Fuentes-Martín, G. Isidori, M. König, N. Selimović, Vector leptoquarks beyond tree level. II. $\mathcal{O}(\alpha_s)$ corrections and radial modes, Phys. Rev. D, vol. 102, no. 3, p. 035021 (2020)
73. A. Greljo, N. Selimovic, Lepton-Quark Fusion at Hadron Colliders, precisely. JHEP **03**, 279 (2021)
74. J. Fuentes-Martín, G. Isidori, M. König, N. Selimović, Vector Leptoquarks Beyond Tree Level. Phys. Rev. D **101**(3), 035024 (2020)
75. M.A. Gigg, P. Richardson, Simulation of Finite Width Effects in Physics Beyond the Standard Model, **5** (2008)
76. D. Berdine, N. Kauer, D. Rainwater, Breakdown of the Narrow Width Approximation for New Physics. Phys. Rev. Lett. **99**, 111601 (2007)
77. V. Bertone, S. Carrazza, N.P. Hartland, J. Rojo, Illuminating the photon content of the proton within a global PDF analysis. SciPost Phys. **5**(1), 008 (2018)
78. R.D. Ball et al., Parton distributions from high-precision collider data. Eur. Phys. J. C **77**(10), 663 (2017)
79. M. Cacciari, G.P. Salam, Dispelling the N^3 myth for the k_t jet-finder. Phys. Lett. B **641**, 57–61 (2006)
80. M. Cacciari, G.P. Salam, G. Soyez, FastJet User Manual. Eur. Phys. J. C **72**, 1896 (2012)
81. A. Alloul, N.D. Christensen, C. Degrande, C. Duhr, B. Fuks, FeynRules 2.0 - A complete toolbox for tree-level phenomenology. Comput. Phys. Commun. **185**, 2250–2300 (2014)
82. A. Bhaskar, D. Das, T. Mandal, S. Mitra, C. Neeraj, Precise limits on the charge-2/3 U1 vector leptoquark. Phys. Rev. D **104**(3), 035016 (2021)
83. A. Bhaskar, T. Mandal, S. Mitra, Boosting vector leptoquark searches with boosted tops. Phys. Rev. D **101**(11), 115015 (2020)
84. A. Bhaskar, T. Mandal, S. Mitra, M. Sharma, Improving third-generation leptoquark searches with combined signals and boosted top quarks. Phys. Rev. D **104**(7), 075037 (2021)
85. CMS Collaboration, Search for scalar leptoquarks produced in lepton-quark collisions and coupled to τ leptons. HEPData (collection), (2023). https://doi.org/10.17182/hepdata.141335
86. G. Aad et al., Search for heavy Higgs bosons decaying into two tau leptons with the ATLAS detector using pp collisions at $\sqrt{s} = 13$ TeV. Phys. Rev. Lett. **125**(5), 051801 (2020)
87. Searches for additional Higgs bosons and vector leptoquarks in $\tau\tau$ final states in proton-proton collisions at $\sqrt{s} = 13$ TeV (2022)
88. J. Aebischer, G. Isidori, M. Pesut, B.A. Stefanek, F. Wilsch, Confronting the vector leptoquark hypothesis with new low- and high-energy data. Eur. Phys. J. C **83**(2), 153 (2023)
89. I. Zurbano Fernandez et al., High-Luminosity Large Hadron Collider (HL-LHC): Technical design report, vol. 10/2020, 12 (2020)
90. C. Cornella, D.A. Faroughy, J. Fuentes-Martin, G. Isidori, M. Neubert, Reading the footprints of the B-meson flavor anomalies. JHEP **08**, 050 (2021)